EuroIntervention 2023;19:e913-e922 published online ahead of print December 2023 ■ published online e-edition December 2023

Intravascular laser lithotripsy for calcium fracture in human coronary arteries

Aleksandra B. Gruslova[1], PhD; Nitesh Katta[2], PhD; Drew Nolen[1], MS; Scott Jenney[2], BS; Deborah Vela[3], MD; Maximilian Buja[3], MD; Mehmet Cilingiroglu[1], MD; Yasamin Seddighi[4], MS; Hai Chao Han[4], PhD; Thomas E. Milner[2], PhD; Marc D. Feldman[1]*, MD

1. Department of Medicine, University of Texas Health, San Antonio, TX, USA; 2. Beckman Laser Institute and Medical Clinic, University of California at Irvine, Irvine, CA, USA; 3. Texas Heart Institute, Houston, TX, USA; 4. Department of Mechanical Engineering, The University of Texas at San Antonio, San Antonio, TX, USA

This paper also includes supplementary data published online at: https://eurointervention.pcronline.com/doi/10.4244/EIJ-D-23-00487

KEYWORDS

- calcified stenosis
- coronary artery disease
- no specific subset
- other technique

Abstract

Background: Electrical intravascular lithotripsy (E-IVL) uses shock waves to fracture calcified plaque.

Aims: We aimed to demonstrate the ability of laser IVL (L-IVL) to fracture calcified plaques in *ex vivo* human coronary arteries and to identify and evaluate the mechanisms for increased vessel compliance.

Methods: Shock waves were generated by a Ho:YAG (Holmium: yttrium-aluminium-garnet) laser (2 J, 5 Hz) and recorded by a high-speed camera and pressure sensor. Tests were conducted on phantoms and 19 fresh human coronary arteries. Before and after L-IVL, arterial compliance and optical coherence tomography (OCT) pullbacks were recorded, followed by histology. Additionally, microcomputed tomography (micro-CT) and scanning electron microscopy (SEM) were performed. Finite element models (FEM) were utilised to examine the mechanism of L-IVL.

Results: Phantom cracks were obtained using 230 µm and 400 µm fibres with shock-wave pressures of 84±5.0 atm and 62±0.4 atm, respectively. Post-lithotripsy, calcium plaque modifications, including fractures and debonding, were identified by OCT in 78% of the *ex vivo* calcified arteries (n=19). Histological analysis revealed calcium microfractures (38.7±10.4 µm width) in 57% of the arteries which were not visible by OCT. Calcium microfractures were verified by micro-CT and SEM. The lumen area increased from 2.9±0.4 to 4.3±0.8 mm^2 ($p<0.01$). Arterial compliance increased by 2.3±0.6 atm/ml ($p<0.05$). FEM simulations suggest that debonding and intimal tears are additional mechanisms for increased arterial compliance.

Conclusions: L-IVL has the capability to increase calcified coronary artery compliance by multiple mechanisms.

**Corresponding author: University of Texas Health at San Antonio, Department of Medicine, Division of Cardiology, 7703 Floyd Curl Drive, DTL 5.532U, San Antonio, TX 78229, USA. E-mail: feldmanm@uthscsa.edu*

© Europa Digital & Publishing 2023. All rights reserved.

SUBMITTED ON 16/06/2023 - REVISION RECEIVED ON 03/09/2023 - ACCEPTED ON 11/10/2023

DOI: 10.4244/EIJ-D-23-00487

Abbreviations

CAC	coronary artery calcification
E-IVL	electrical intravascular lithotripsy
FEM	finite element model
L-IVL	laser intravascular lithotripsy
OCT	optical coherence tomography
PCI	percutaneous coronary intervention
SEM	scanning electron microscopy

Introduction

Coronary artery calcification (CAC) complicates percutaneous coronary intervention (PCI) by reducing vessel compliance, interfering with device delivery, impairing balloon expansion, and possibly causing uneven drug distribution in the arterial wall[1]. Furthermore, CAC causes damage to the drug-eluting polymer, resulting in a higher rate of treatment failure[2]. Decreased vessel compliance also reduces the expansion of implanted stents, which can lead to stent failure as well as complications such as stent thrombosis and restenosis[3]. Calcium localisation (superficial or deep), distribution (focal, circumferential or longitudinal extension) and thickness also adversely impact procedural time and success[4]. CAC is an independent predictor of a lower survival rate and is strongly correlated with major adverse cardiovascular events (MACE) post-PCI[5].

Given the significant challenges calcium presents in PCI, a variety of therapeutic devices have been developed over the past several decades[1,6-9]. These devices utilise one or more of three energy mechanisms: mechanical, electrical, and optical. Mechanical devices (e.g., cutting balloons with microsurgical blades) increase luminal area greater than plain old balloon angioplasty (POBA) and, therefore, increase compliance. However, these cutting procedures cannot reach calcium located deep in the vessel wall[6]. Rotational and orbital atherectomy devices utilise a rotating tip with abrasive diamonds that cut tissue and reshape the calcific atherosclerotic lesion[10]. These devices debulk plaque but can only remove superficial calcium. Moreover, mechanical atherectomy devices do not greatly increase vessel compliance[6,10], and use of these devices carries a risk of no-reflow and vessel perforation[7]. Electrical intravascular lithotripsy (E-IVL) uses an electrical discharge to generate ultrasonic waves which crack calcium deep in the arterial wall without material removal, leaving soft tissue intact[9]. However, E-IVL is limited in the treatment of coronary arteries. The smallest E-IVL catheter diameter is 0.047" (1.2 mm), therefore, it is challenging to cross many calcified lesions that have a mean lumen diameter of 0.8 mm (Salem et al. The mechanism of balloon uncrossability assested by intravacular ultrasound. J Am Coll Cardiol. 2020;75:1447). Atherectomy is sometimes performed prior to E-IVL to provide coronary access for lithotripsy, adding time and cost to PCI procedures and increasing the risk of no-reflow.

High-energy laser pulses can be delivered through a catheter via a small diameter (e.g., 50 µm) silica optical fibre[11] compatible with small balloon profiles. Optical fibres can be incorporated into commercial low-profile, lubricious balloons. E-IVL uses thicker and less compliant balloons to minimise the chance of balloon rupture due to electric arcing. Furthermore, in laser-based IVL (L-IVL), shorter laser pulses can result in higher pressure amplitude generation at similar pulse energies[12]. Ultrashort electric pulse generation is challenging because of the high impedance of transducing high voltage pulses along small diameter wires. Thus, L-IVL provides some advantages over E-IVL.

Herein, we present the first study of L-IVL. Bench-top experiments were conducted to verify that acoustic pressure amplitudes

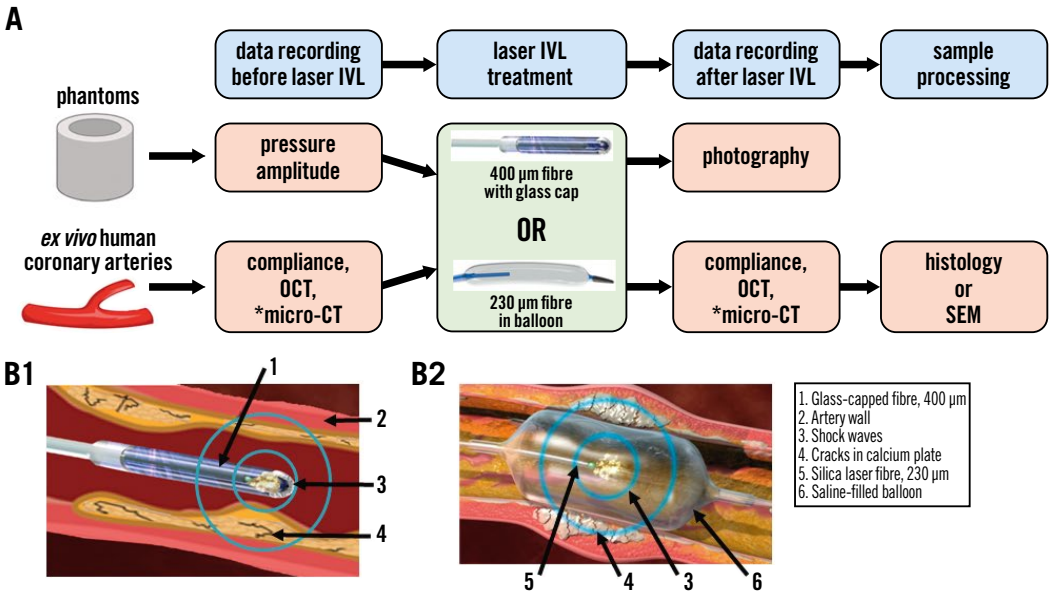

Figure 1. *Laser IVL study design. A) Graphical representation of the experimental design (*selected arteries). B) Cross-sectional images of the laser IVL catheter: (B1) 400 µm optical fibre with glass cap, (B2) 230 µm optical fibre in balloon. CT: computed tomography; IVL: intravascular lithotripsy; OCT: optical coherence tomography; SEM: scanning electron microscopy*

are generated by the collapse of laser-induced cavitation bubbles in saline. *Ex vivo* studies were conducted on human calcified coronary arteries. Various imaging techniques, including optical coherence tomography (OCT), histopathology, microcomputed tomography (micro-CT), and scanning electron microscopy (SEM), were performed to verify that calcium plate microfractures had occurred, and to identify and evaluate any additional mechanisms of increased vessel compliance. Finite element model (FEM) studies evaluated the contribution of debonding and intimal tears to increased vessel compliance **(Supplementary Appendix 1)**.

Methods

The present study was first conducted on phantoms simulating coronary artery calcification. After the laser-based lithotripsy was validated on phantoms and the pressure amplitude was determined, the study was carried out on fresh *ex vivo* calcified coronary arteries. A graphical representation of the experiments is shown in **Figure 1**.

BENCH-TOP STUDIES

PHANTOM PREPARATION

Solid phantoms (3-5 mm inner diameter [ID], 2 cm length, 1-2 mm wall thickness) were made from plaster of Paris (DAP Products Inc.), and Ultracal 30 (Capital Ceramics) with fixed powder/water ratios of 2:1 and 100:38, respectively,[13] to validate L-IVL. We constructed 30% gelatin phantoms (gelatin, G2625, Sigma-Aldrich) with two embedded BegoStone (BEGO USA; powder/water ratio 5:1)[14] plates (3 cm, 1 mm thickness) to mimic a vessel wall containing calcifications.

LASER LITHOTRIPSY

Experiments were performed with a Ho:YAG (Holmium: yttrium-aluminium-garnet) laser (Lumenis Pulse 120H, λ=2.1 µm; Boston Scientific) at a fixed 5 Hz pulse frequency and a 70 µs pulse duration. Two sizes of silica optical fibres (400 µm [glass capped] and 230 µm [in balloon]; MED-Fibers) were centred inside phantoms that were fully submerged in saline.

PRESSURE MEASUREMENTS

Shock-wave pressure amplitude profiles were recorded by a high-frequency pressure sensor (active diaphragm diameter 0.218"; PCB Piezotronics). The optical fibre was oriented at 90° to the normal axis of the pressure sensor at a separation distance of 3 mm. Recorded pressure amplitude profiles were calculated for a 1 mm separation distance to simulate an *in vivo* application.

DEMONSTRATION OF EQUIVALENT PRESSURE GENERATION OF AN OPTICAL FIBRE WITH OR WITHOUT BALLOON MATERIAL

Pressure amplitudes generated by the 400 µm optical fibre were tested with non-compliant balloon material (Pebax; Biomerics), used for our L-IVL catheter balloon, and with a contemporary E-IVL balloon (Shockwave Medical). Both measurements were compared with the pressure generated by the optical fibre submerged in saline without balloon material. The balloon material was placed both in direct contact with and at a distance of 3 mm from the pressure sensor surface, to mimic direct contact or the distance between the balloon and the vessel wall, respectively. The balloon wall thickness (30 µm) was identical for both L-IVL and E-IVL materials.

EX VIVO HUMAN ARTERIES

Following the validation of L-IVL in phantoms, 11 fresh *ex vivo* human hearts were obtained. All coronary arteries were utilised within 24 hours of death. This study was approved by the institutional review board of the South Texas Blood & Tissue Center.

OPTICAL COHERENCE TOMOGRAPHY IMAGE ACQUISITION AND ANALYSIS

Ex vivo coronary arteries were evaluated using the ILUMIEN OPTIS OCT System and Dragonfly Imaging Catheter (Abbott). Calcified plaque was identified in OCT images as a highly attenuated signal with sharply delineated borders. Areas with calcified lesions were denoted with a tissue-marking dye (Mart-It; McKesson) on the outside of the vessel wall. Using recorded OCT images, the calcium arc, length, thickness, lumen area (before and after L-IVL), and calcium score were determined in the treatment area **(Supplementary Table 1)**.

MEASUREMENT OF ARTERIAL COMPLIANCE

The lumen diameter was determined by OCT, and compliance was measured before and after L-IVL using an inflation device (Merit Medical) and a balloon catheter (Medtronic) that matched the lumen diameter (1:1). First, baseline balloon compliance was measured in the air. Starting from zero-gauge pressure, saline was injected into the balloon at constant volume increments of 0.25 mL. Pressure values were recorded at each volume (from 0 to 2.5 mL). Measurements were stopped before the specified balloon burst pressure was reached. Next, the balloon was inserted into the arterial region with significant calcification. Measurements were performed in triplicate, before and after L-IVL treatment.

LASER LITHOTRIPSY TREATMENT

A set of *ex vivo* arteries (n=4, from 4 hearts) were treated with a 230 µm optical fibre in a balloon (3 mm x 20 mm) filled with saline and pressurised at 4 atm. Fifteen *ex vivo* arteries (7 hearts) were treated with 400 µm optical fibres with glass caps. Each artery was submerged in saline, and the optical fibre was positioned within the marked calcified area using an aiming beam. Shock waves were generated by a Ho:YAG laser at a fixed 5 Hz pulse frequency and 2 J of energy. On average, 30 and 100 laser pulses (glass-capped optical fibre and fibre in balloon, respectively) were applied per 10 mm of arterial length.

HISTOLOGY, COREGISTRATION WITH OCT IMAGES AND ANALYSIS

Arteries were fixed in 10% formalin and radiographed with a Faxitron MX-20 (Faxitron Bioptics LLC). All arteries were immersed in decalcifying solution (Epredia Cal-Rite; Fisher Scientific) for 12-24 hours. Arteries were sliced into 2-3 mm rings (~15 rings/artery) and processed for paraffin-embedding (Sakura Finetek). Sections of 5 µm were cut at 150 µm intervals and stained with haematoxylin and eosin (H&E). The OCT frames

and histological sections were coregistered using anatomical landmarks (e.g., side branches, calcification sites, lumen geometry) and external tissue-dye markings. The fracture width was measured at three locations along the length of the fracture and averaged.

MICROCOMPUTED TOMOGRAPHY

Selected *ex vivo* arteries were scanned before and after L-IVL with a desktop micro-CT system (SkyScan 1173; Bruker) equipped with a microfocus X-ray tube with a 5 µm spot size, using a 20 µm isotropic voxel size, 60 kV, 167 µA, and a 0.5 mm aluminium filter. Specimens were affixed to a plastic specimen holder filled with cold saline. As the artery was not cut, micro-CT was able to show calcified plaque architecture.

SCANNING ELECTRON MICROSCOPY

Samples were fixed with McDowell Trump's fixative (Electron Microscopy Sciences) and subsequently incubated in 10% NaOH solution for 6-10 days − 1% tannic acid and mixture of 1% OsO4 in 0.1 M sodium cacodylate buffer, modified from Stephenson et al[15]. After dehydration in a series of alcohol solutions, a plastic embedding protocol was used to preserve the calcified plaque architecture[16]. Before imaging, segments were coated with a layer of gold (Au) using a PELCO SC-7 unit (PELCO). Images were acquired at 5 keV using a ZEISS Crossbeam 340 SEM (ZEISS) equipped with an Oxford X-Max SDD X-ray detector (Energy-Dispersive Spectroscopy; Oxford Instruments) for the identification of chemical constituents.

FINITE ELEMENT MODELLING OF COMPLIANCE PRE- AND POST-L-IVL

Histological images of the arteries were used to generate FEMs to analyse the relationship of lumen area to pressure. While treated images showed calcium plate modifications, intact and partial intact cross-sections were recreated by removing all or some fractures in the calcium plate images. The two-dimensional (2D) cross-sections were extended longitudinally for 3 mm to create three-dimensional (3D) models. Both the arterial wall and calcifications were assumed to be isotropic, incompressible, and hyperelastic material with a polynomial strain energy density function[17]. Details of the arterial wall and plaque material coefficients can be found in **Supplementary Table 2**. Simulation of the pressurised inflations were performed using FEM software ABAQUS (Dassault Systèmes Simulia Corp).

STATISTICAL ANALYSIS

Continuous variables are expressed as mean±standard deviation (SD). A paired t-test was used to compare the difference between pre- and post-treatment of the same artery. The Pearson correlation coefficient was computed to test correlation between two variables. A value of $p<0.05$ was considered statistically significant.

Results

LASER-INDUCED ULTRASONIC PRESSURE WAVE GENERATION

Upon pulsed-laser irradiation, the light-saline interaction creates a vapour bubble **(Figure 2A, Figure 2B)**. The collapse of the vapour bubble **(Figure 2C, Figure 2D)** generates a shock wave. Pressure versus time data in response to a single pulse (2 J, 5 Hz) achieved 62.0±0.4 atm and 84.0±5.0 atm with 400 µm and 230 µm fibres, respectively **(Figure 2E)**.

Pressure amplitude measurements with and without L-IVL balloon material showed that the L-IVL non-compliant balloon material did not attenuate the pressure wave. A single laser pulse emitted by a 400 µm fibre reached a pressure of 61.6±2.5 atm for L-IVL non-compliant balloon material versus 61.5±2.9 atm for Shockwave Medical's balloon material (n=5 for both; p=0.12). No difference in pressure amplitude was observed when the balloon material did or did not contact the pressure sensor surface (L-IVL balloon: 61.6±2.5 atm vs 66.3±5.6 atm; p=0.12; E-IVL balloon: 61.5±2.9 atm vs 63.3±2.1 atm; p=0.29, respectively). Due to equivalent pressure

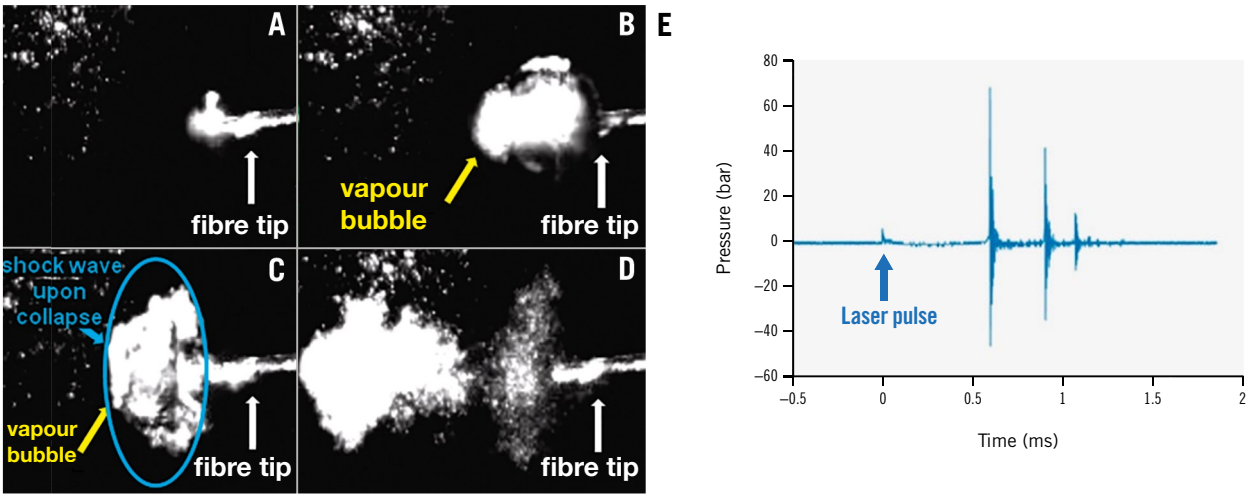

Figure 2. *Mechanism of laser-based IVL. A,B) Bubble formation in saline. C,D) Bubbles collapse, generating a sonic pressure wave. E) Pressure versus time data measured with a pressure sensor after a single pulse at the same setting used for the phantom and ex vivo artery experiments (2 J, 70 µs pulses). IVL: intravascular lithotripsy*

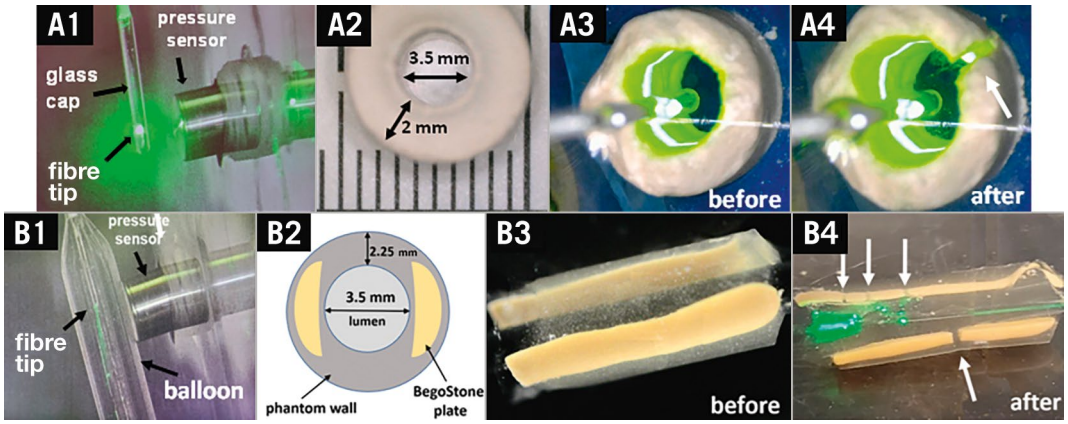

Figure 3. *Laser lithotripsy in calcium phantoms. A) 400 µm optical fibre with a glass cap: (A1) pressure measurement set up, (A2) plaster of Paris phantom, (A3) phantom before L-IVL, (A4) phantom after L-IVL. B) 230 µm optical fibre in a balloon: (B1) pressure measurement set up, (B2) cross-sectional diagram of gelatin phantom with two BegoStone plates, (B3) phantom before L-IVL, (B4) phantom after L-IVL. Fractures are labelled with white arrows. L-IVL: laser intravascular lithotripsy*

amplitude generation through both balloon materials and the challenges in custom prototyping L-IVL balloons for arteries with variable lumen diameters, many of the results presented below were performed with glass-capped optical fibres without a balloon.

BENCH-TOP STUDY WITH PHANTOMS

Various phantoms were constructed to validate the ability of L-IVL to generate a shock wave with amplitude sufficient to fracture calcium. Plaster of Paris cylindrical phantoms (n=6) developed fractures due to L-IVL with a 400 µm glass-capped fibre at 2 J pulse energy **(Figure 3A)**. Ultracal 30 phantoms presented a higher fracture threshold than plaster of Paris phantoms due to the higher bulk modulus of water/Ultracal 30 mixtures at the ratio 100:38[13]. Ultracal 30 phantoms (n=6) were fractured on average after 125±25 pulses, with the highest fluence rate achieved in 230 µm fibres, with 2 J pulse energy and 70 µs pulse duration (greater than 70 atm).

Gelatin phantoms (3.5 mm ID) with embedded BegoStone plates simulated a soft vessel wall with hard calcium plates **(Figure 3B)**. Fractures in embedded BegoStone plates were created in all phantoms (n=4) using a 230 µm fibre (2 J, 5 Hz) in a balloon (3.5 mm) pressurised at 4 atm. Fractures were detected with photography and were visible perpendicular to the optical fibre orientation **(Figure 3B4)**.

EX VIVO HUMAN CORONARY ARTERIES

Baseline OCT assessment showed an average calcium arc, thickness and length in the target area of 145.3±40.60°, 0.8±0.3 mm, and 5.3±1.9 mm, respectively, indicating significant calcification **(Figure 4A)** (n=19 arteries, n=11 hearts). The treatment was conducted in a pre-marked calcified area based on OCT **(Figure 4B)**. Measurements of the laser power before and after L-IVL treatment showed no change (8.2±0.7 W and 8.3±0.6 W, respectively; p=0.85), suggesting consistent shock-wave amplitudes were delivered to treated arteries.

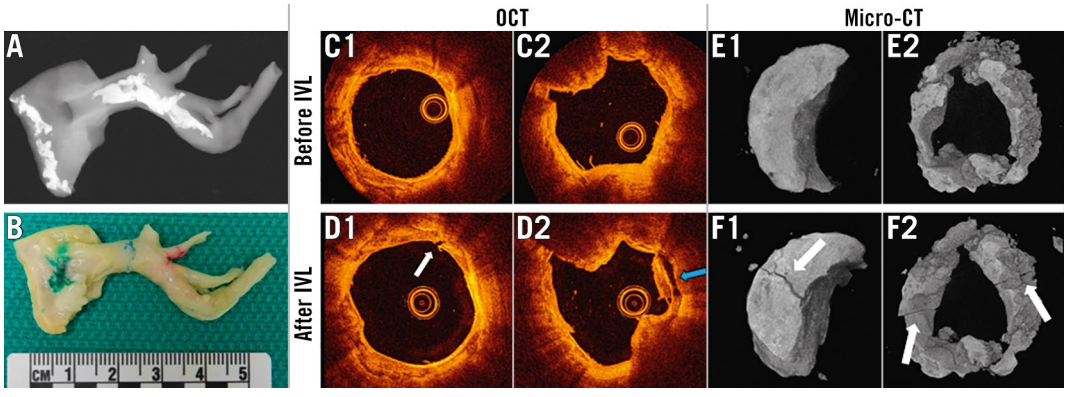

Figure 4. *L-IVL experiments in ex vivo human coronary arteries with a 230 µm optical fibre in a balloon. A) X-ray of the artery before histological processing, confirming the presence of calcification in the treatment area. B) Dissected human coronary artery with calcified region marked in blue. Green and red marks denote the proximal and distal ends of artery. C-D) Representative OCT images before (C) and after L-IVL (D). White arrows indicate fracture, the blue arrow the debonding of the calcium plate/non-calcium plate junction. E-F) Representative micro-CT images before L-IVL (E) and after L-IVL (F). CT: computed tomography; L-IVL: laser intravascular lithotripsy; OCT: optical coherence tomography*

STUDIES WITH A LASER FIBRE IN A BALLOON

Four arteries from 4 hearts were treated with a 230 µm optical fibre in a balloon inflated to 4 atm pressure **(Figure 3B1)**, which demonstrated fractures of calcified plaque on OCT **(Figure 4C, Figure 4D)** and micro-CT images **(Figure 4E, Figure 4F)**. The lumen area measured by OCT before and after treatment increased from 4.6±3.3 mm^2 to 5.5±2.8 mm^2 (n=4; p=0.05).

STUDIES WITH A GLASS-CAPPED LASER FIBRE

Fifteen arteries from 7 human hearts were treated with a 400 µm glass-capped laser fibre **(Figure 3A1)**. Comparison of OCT pullbacks before and after treatment showed that L-IVL led to a significant increase in lumen area (from 2.9±0.4 mm^2 to 4.3±0.8 mm^2, n=15; p=0.038) that was observed in 87% of treated arteries **(Figure 5A)**. Analysis of OCT pullbacks did not show a significant correlation between the calcium score and the change in lumen area (corr.=0.12; p=0.653). These data are consistent with an increase in artery lumen area regardless of calcium score. A significant increase in compliance was observed after L-IVL in 53% of arteries (p<0.05) **(Figure 5B)**. In addition, a comparison of balloon compliance in the air before and after *ex vivo* experiments confirmed that no changes in balloon compliance occurred that might artificially impact measurements of arterial compliance **(Supplementary Figure 1)**.

After L-IVL, OCT-observed modifications included calcium plate fractures and debonding in 15 arteries (78%) **(Figure 5C, Figure 5D)**. On average 3.4±2.3 fractures were observed per targeted 10 mm lesion. Multiple (2 to 3) calcium fractures on a single OCT frame were identified in 26% of treated arteries. The width and depth of the calcium fractures were 0.32±0.18 mm and 0.47±0.31 mm, respectively. Calcium fractures following L-IVL were also confirmed with micro-CT **(Figure 5E)**.

Histopathological evaluation of the arteries after L-IVL revealed calcium microfractures in 57% of treated arteries, which were not all visible with OCT **(Figure 6)** possibly due to a deep position of the calcium plates and limited light penetration. These microfractures were located in both superficial and deep calcium plates (from 0.14 mm to 1.84 mm). The thickness of calcium microfractures was 38.7±10.4 µm, and the depth of calcium plates was 1,743.3±939.5 µm. A detailed analysis of H&E sections showed that microfractures were associated with debonding of the calcium plate (30%), while 5% of the sections had microfractures only. Coregistration of histological images with micro-CT confirmed microfractures **(Figure 6B)**.

To better understand the relationship between calcium plate fracture, calcium microfracture, and debonding, SEM of calcified arteries was performed. The protocol was developed to eliminate artefacts during sample processing and to provide qualitative information about calcium plate and collagen fibrous interaction. As demonstrated in **Figure 7**, calcium microfractures and debonding are both apparent in the region of thickest calcium. Calcium plate composition was confirmed with X-ray spectroscopy **(Supplementary Figure 2)**.

RELATIVE CONTRIBUTION OF CALCIUM FRACTURE, DEBONDING, AND INTIMAL TEARS IN IMPROVING ARTERIAL COMPLIANCE

Different FEMs derived from histology, which included intact arterial components, calcium fractures, debonded calcium plate/non-calcium plate interfaces, and intimal tears, were analysed to

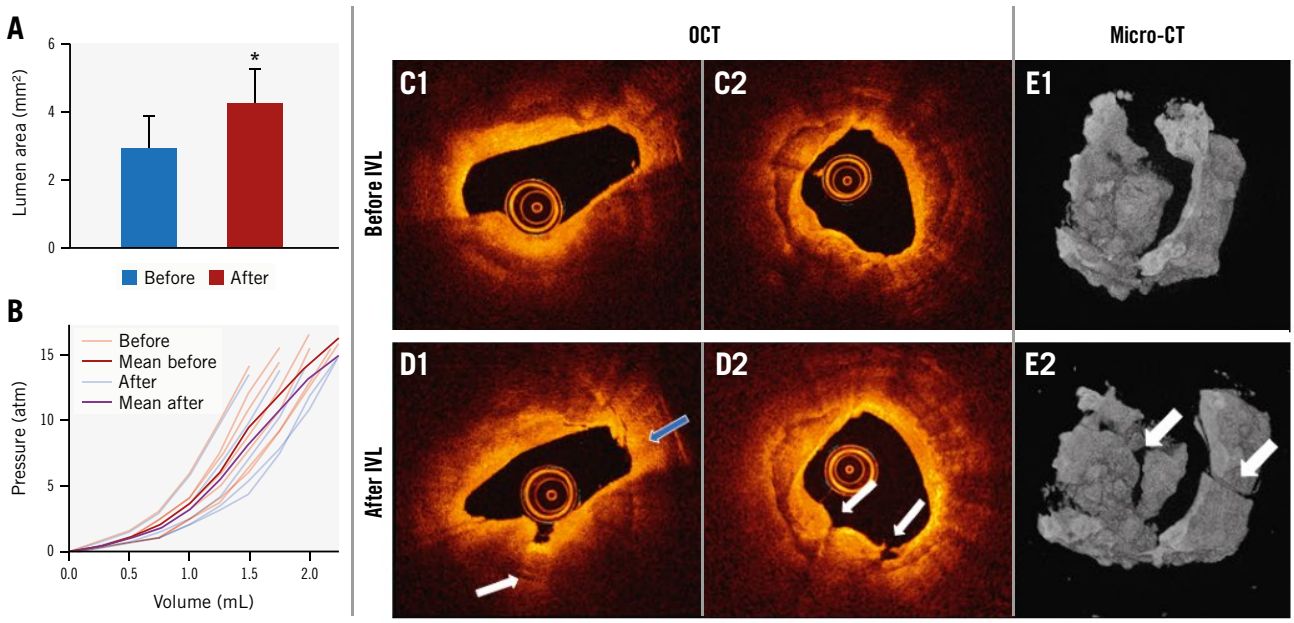

Figure 5. *L-IVL experiments in ex vivo human coronary arteries with a 400 µm optical fibre with a glass cap. A) Average lumen area before and after L-IVL (p=0.038). B) Spaghetti plot of ex vivo artery compliance at given volumes before and after L-IVL (p<0.05). C) Representative OCT images before L-IVL. D) OCT images after L-IVL (white arrows indicate calcium fractures, the blue arrow the debonding of the calcium plate). E) Representative micro-CT images before (E1) and after (E2) L-IVL. CT: computed tomography; L-IVL: laser intravascular lithotripsy; OCT: optical coherence tomography*

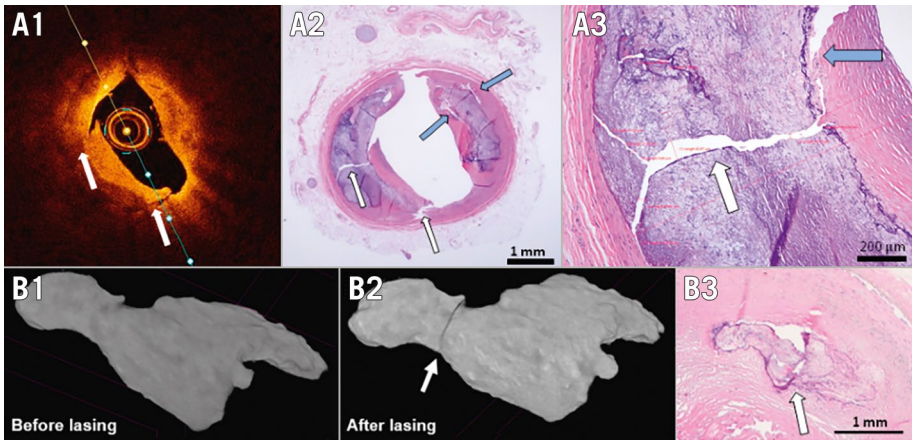

Figure 6. *Representative examples of calcium plaque modifications induced by L-IVL. A) Optical coherence tomography images after L-IVL treatment (A1) were coregistered with histological sections stained with H&E at 4x (A2) and at 25x (A3) magnification (white arrows indicate calcium fracture, the blue arrows show the debonding of calcium plate and red lines represent measurements of calcium fractures). B) Longitudinal micro-CT scans of calcified ex vivo coronary artery segment before (B1) and after (B2) laser IVL, and coregistered histological cross-section (B3). CT: computed tomography; H&E: haematoxylin and eosin; L-IVL: laser intravascular lithotripsy*

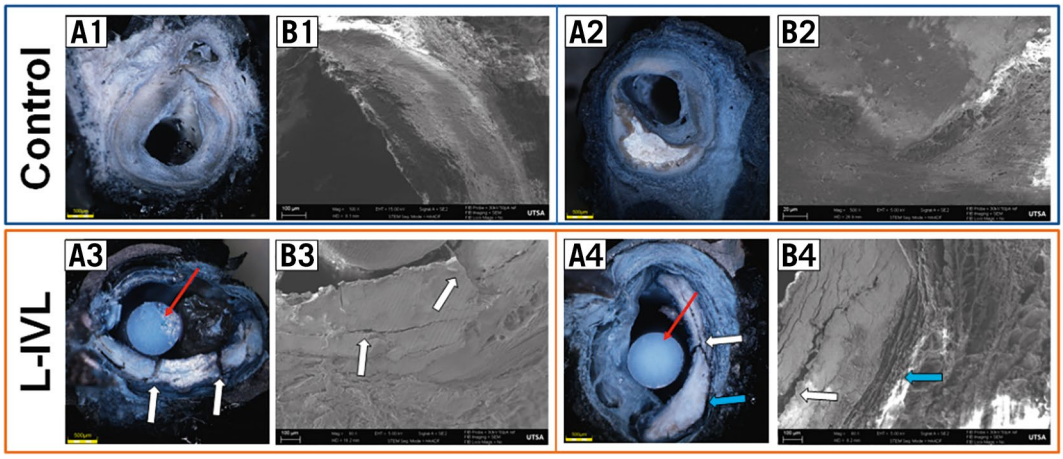

Figure 7. *SEM demonstrating calcium plate fracture and debonding at the calcium plate/non-calcium plate junction in response to L-IVL. A) Cross-sectional view of an ex vivo coronary SEM sample after plastic embedding protocol: A1,A2) control samples, A3,A4) after L-IVL with a 230 µm laser fibre in a balloon. B1-B4) SEM images of a magnified region of the calcium plate (white arrows indicate calcium plate fracture, blue arrows show debonding, red arrows are plastic sticks used for embedding sample): B1, B2) control samples, B3, B4) after L-IVL. L-IVL: laser intravascular lithotripsy; SEM: scanning electron microscopy*

determine the relative contribution of mechanisms that increase vessel compliance **(Figure 8)**. Changes in the lumen area of the calcified coronary artery were calculated versus lumen pressure to give vessel compliance **(Figure 8B)**. FEM simulation results suggest that fractures in calcium plates alone had a minor contribution to increasing vessel compliance, and compliance increases with greater numbers of fractures. Debonding and intimal tears contributed more to increasing arterial compliance than calcium fractures alone **(Figure 8BD, Figure 8BE, Figure 8BF)**.

Discussion

An effective treatment for calcium is motivated by the clinical objective to fully expand a stiff arterial wall **(Central illustration)**. The presence of heavily calcified coronary lesions can be overwhelming and result in incomplete stent deployment, resulting in "stent regret" with adverse outcomes[2]. In such cases, more sophisticated methods of calcium remodelling are required. Therefore, a new balloon-based approach for the treatment of severe arterial calcification using pulsatile sonic pressure waves was successfully adopted into practice[9]. However, despite the success in safely cracking calcium within the vessel wall by E-IVL, some coronary lesions remain uncrossable due to catheter profiles of 1.2 mm. In fact, atherectomy is sometimes performed prior to E-IVL to provide coronary access for lithotripsy, which increases the time and cost of the PCI procedure and still increases the risk to the patient of the no-reflow phenomenon.

The initial use of excimer lasers without balloons in the 1990s to vaporise plaque had a high complication rate due to uncontrolled microcavitations in blood with contrast. The safety of excimer laser has been proven for calcified coronary plaque fracture when lasing

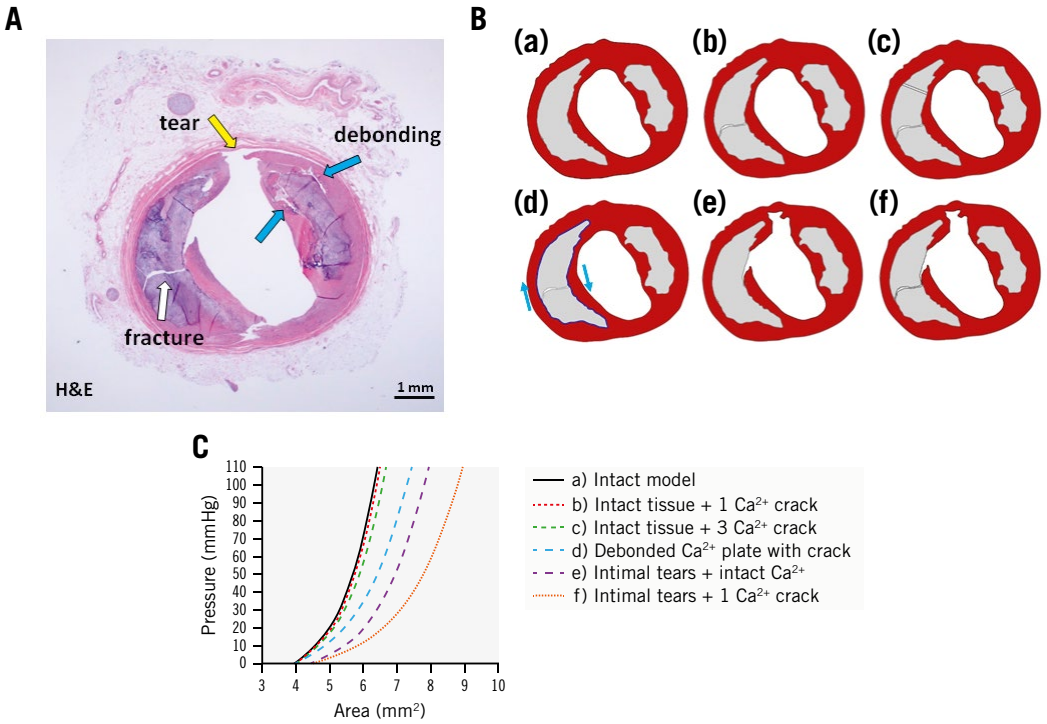

Figure 8. *Effect of calcium plate modifications on coronary artery compliance determined by finite element model (FEM). A) Cross-sectional image of artery after L-IVL treatment (H&E). Ba-Bf) Six FEM models to compare the relative importance of calcium plate fracture, debonding, and intimal tears on improving vessel compliance. C) Lumen area plotted as function of lumen pressure for these models. Ca^{2+}: calcium; FEM: finite element model; H&E: haematoxylin and eosin; L-IVL: laser intravascular lithotripsy*

EuroIntervention

CENTRAL **ILLUSTRATION** **Laser-based intravascular lithotripsy (L-IVL) modifies calcium plates in coronary arteries.**

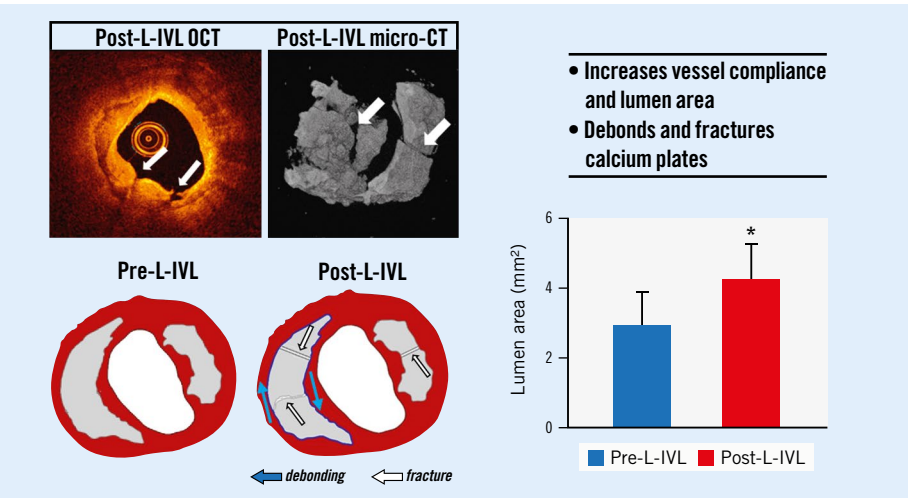

L-IVL in ex vivo human coronary arteries shows successful calcium treatment (OCT, micro-CT) leading to increased lumen area and compliance due to calcium fracture and debonding. CT: computed tomography; OCT: optical coherence tomography

in saline[8]. Optical fibres were first placed in balloons by Spears et al[18] to weld coronary dissections – although this approach failed due to heat-induced vessel constriction. Greater safety is expected for L-IVL, since microcavitations are contained within a balloon, thus mitigating misdirected pressure wave generation and non-specific thermal injury. Although lasers can transmit large pulse energies (~2 J) over very small fibre cross-sections (~50 µm), no U.S. Food and Drug Administration (FDA)-approved L-IVL device exists.

Navigation of the laser balloon to the calcified region to be treated with laser IVL is identical to the placement of any balloon during percutaneous transluminal coronary angioplasty. Lasers have temporal design advantages over electricity for shock-wave generation. Increasing the laser fluence rate by decreasing pulse duration maintains the same energy and can result in greater pressure amplitude generation[19]. Smaller diameter fibres can also deliver greater fluence rates than large diameter fibres, providing a spatial design advantage for lasers over electricity. Our study demonstrated that L-IVL can achieve higher peak pressures (200 atm, data not shown) than values reported for E-IVL (50 atm in coronaries and 100 atm in peripheral vessels)[9]. Our study demonstrates the ability of L-IVL to fracture calcium in solid phantoms and *ex vivo* human coronary arteries. L-IVL, when treating calcified *ex vivo* coronary arteries, increases both lumen area and arterial compliance. L-IVL fracture of both deep and superficial calcium plates was confirmed with OCT, histology, micro-CT and SEM.

Despite the demonstrated safety of E-IVL in multiple clinical trials, asynchronous ventricular pacing can occur. Two reports of ventricular fibrillation were entered into the FDA's MAUDE database, and a third case was published[20], as well as three reports of atrial fibrillation/flutter[21-23]. Given the high number of patients treated with E-IVL, safety has not been a concern. The mechanism of pacing is unclear: electric pacing is one mechanism, but reports suggest ultrasonic waves can result in ion channel current modulation. The tetrodotoxin-resistant Nav1.5 channel is the most common Na^+ channel isoform in cardiomyocytes, and previous studies have demonstrated the mechanical sensitivity of this channel[24,25]. If the latter is a mechanism, then L-IVL may also result in ventricular pacing, although further studies are required. Interestingly, no known reports of laser-induced cardiac pacing exist despite decades of use of coronary laser atherectomy.

In the 1990s, publications of *in vivo* balloon angioplasty of calcified coronary arteries examined with intravascular ultrasound demonstrated that arterial dilation at the angioplasty site occurred due to dissection at the calcium plate/non-calcium plate junction[26]. In our study, we observed not only the expected calcium plate fractures in response to L-IVL, but also separation between the calcium plate and the non-calcium plate interface, which we term "debonding". The relative contribution of calcium fracture, debonding, and intimal tear mechanisms for increasing arterial compliance was investigated by FEM simulations. The impact of separating atherosclerotic tissue adjacent to the calcium plate – or debonding – is shown to improve arterial compliance by FEM **(Figure 8)**.

Recent studies using X-ray diffraction demonstrate that fibrous tissue in atherosclerotic plaque is oriented circumferentially but becomes more longitudinally directed as it transitions toward attachment to a calcium plate[27]. Stress depends upon fibril orientation, with the greatest tissue stress in the longitudinal direction of collagen fibrils[28]. The geometry of fibrous calcified plaque interfaces can amplify stresses near the lesion interface[29]. Therapeutic procedures that separate the calcium plate/fibrous tissue interfaces can relieve residual stress and may contribute to improved coronary arterial compliance to a greater extent than calcium plate fractures alone.

Arterial lithotripsy may utilise a previously unrecognised mechanism – debonding – for increasing arterial compliance and treating atherosclerotic plaque. Moreover, excimer and E-IVL clinical efficacy may support our FEM simulation results for observed improvement of arterial compliance. FEM results also suggest that calcium plate fractures alone did not result in a significant improvement of arterial compliance. The addition of debonding and intimal tears did improve arterial compliance in combination with calcium plate fracture. By better understanding the underlying mechanical mechanisms, modifications in energy delivery to the vessel wall may further improve clinical outcomes.

Limitations

There are concerns related to L-IVL which were not addressed in the current study. We have achieved a pressure amplitude of up to 200 atm. Shockwave Medical E-IVL achieves 50 atm in clinical practice. There is no literature detailing how many atmospheres generated by IVL can cause arterial perforation. There is a similar concern for the number of IVL pulses delivered. We delivered over 10 pulses/sec without damage to the balloon; however, we have not yet delivered 10 pulses/sec to an *ex vivo* coronary artery. Shockwave Medical IVL coronary catheters deliver 1 pulse/sec. The impact of the high pulse rate available with laser is not currently known. Finally, it is unknown whether laser IVL causes myocardial pacing similar to that seen with Shockwave Medical E-IVL.

Conclusions

We demonstrated that L-IVL can expand the development of sonic-based interventional devices for the treatment of calcified coronary arteries. We have presented the advantages of L-IVL and identified new mechanisms in shock wave approaches to increase arterial compliance.

Impact on daily practice

E-IVL has advanced the field of treatment of calcified coronary arteries. However, limitations persist such as concerns over crossability due to the profile of wires and electrodes. L-IVL allows miniaturisation of the lithotripsy source, solving the problem of the crossing profile. Translation of our results into patient care will expand the lesion subset who are treatable with IVL without preprocedural plaque modification.

Funding

This work is supported by the Clayton Foundation for Biomedical Research (Houston, TX, USA), NIH RO1 HL 163582-01, a seed grant from the Office of Vice President for Research, University of Texas at San Antonio, and a Postdoctoral Fellowship to Nitesh Katta, PhD, from the American Society for Lasers in Surgery and Medicine.

Conflict of interest statement

A.B. Gruslova, N. Katta, D. Nolen, S. Jenney, T.E. Milner, and M.D. Feldman had salary support from the Clayton Foundation for Research. The other authors have no conflicts of interest to declare.

References

1. Barbato E, Shlofmitz E, Milkas A, Shlofmitz R, Azzalini L, Colombo A. State of the art: evolving concepts in the treatment of heavily calcified and undilatable coronary stenoses – from debulking to plaque modification, a 40-year-long journey. *EuroIntervention.* 2017;13:696-705.

2. Hendry C, Fraser D, Eichhofer J, Mamas MA, Fath-Ordoubadi F, El-Omar M, Williams P. Coronary perforation in the drug-eluting stent era: incidence, risk factors, management and outcome: the UK experience. *EuroIntervention.* 2012;8:79-86.

3. Park JH, Sohn IS, Jin ES, Cho JM, Kim CJ, Lee YK. Heavy coronary calcium mimicking in-stent restenosis. *Korean Circ J.* 2011;41:421.

4. Lee MS, Shah N. The Impact and Pathophysiologic Consequences of Coronary Artery Calcium Deposition in Percutaneous Coronary Interventions. *J Invasive Cardiol.* 2016;28:160-7.

5. Williams MC, Moss AJ, Dweck M, Adamson PD, Alam S, Hunter A, Shah ASV, Pawade T, Weir-McCall JR, Roditi G, van Beek EJR, Newby DE, Nicol ED. Coronary Artery Plaque Characteristics Associated With Adverse Outcomes in the SCOT-HEART Study. *J Am Coll Cardiol.* 2019;73:291-301.

6. Shah M, Najam O, Bhindi R, De Silva K. Calcium Modification Techniques in Complex Percutaneous Coronary Intervention. *Circ Cardiovasc Interv.* 2021;14:e009870.

7. Barrett C, Warsavage T, Kovach C, McGuinn E, Plomondon ME, Armstrong EJ, Waldo SW. Comparison of rotational and orbital atherectomy for the treatment of calcific coronary lesions: Insights from the VA clinical assessment reporting and tracking (CART) program. *Catheter Cardiovasc Interv.* 2021;97:E219-26.

8. Tsutsui RS, Sammour Y, Kalra A, Reed G, Krishnaswamy A, Ellis S, Nair R, Khatri J, Kapadia S, Puri R. Excimer Laser Atherectomy in Percutaneous Coronary Intervention: A Contemporary Review. *Cardiovasc Revasc Med.* 2021;25:75-85.

9. Karimi Galougahi K, Patel S, Shlofmitz RA, Maehara A, Kereiakes DJ, Hill JM, Stone GW, Ali ZA. Calcific Plaque Modification by Acoustic Shock Waves: Intravascular Lithotripsy in Coronary Interventions. *Circ Cardiovasc Interv.* 2021;14:e009354.

10. Kaul A, Dhalla PS, Bapatla A, Khalid R, Garcia J, Armenta-Quiroga AS, Khan S . Current Treatment Modalities for Calcified Coronary Artery Disease: A Review Article Comparing Novel Intravascular Lithotripsy and Traditional Rotational Atherectomy. *Cureus.* 2020;12:e10922.

11. Blackmon RL, Hutchens TC, Hardy LA, Irby PB, Fried NM. Characterization of a 50-µm m-Core Optical Fiber for Potential use in Thulium Fiber Laser Lithotripsy. In: Choi B, Kollias N, Zeng H, et al., eds. Proceedings of SPIE; SPIE, USA; 2014:89261F.

12. Jansen ED, Asshauer T, Frenz M, Motamedi M, Delacrétaz G, Welch AJ. Effect of pulse duration on bubble formation and laser-induced pressure waves during holmium laser ablation. *Lasers Surg Med.* 1996;18:278-93.

13. Esch E, Simmons WN, Sankin G, Cocks HF, Preminger GM, Zhong P. A simple method for fabricating artificial kidney stones of different physical properties. *Urol Res.* 2010;38:315-9.

14. Liu Y, Zhong P. BegoStone--a new stone phantom for shock-wave lithotripsy research. *J Acoust Soc Am.* 2002;112:1265-8.

15. Stephenson MK, Lenihan S, Covarrubias R, Huttinger RM, Gumina RJ, Sawyer DB, Galindo CL. Scanning Electron Microscopy of Macerated Tissue to Visualize the Extracellular Matrix. *J Vis Exp.* 2016:54005.

16. Mukhamadiyarov RA, Bogdanov LA, Glushkova TV, Shishkova DK, Kostyunin AE, Koshelev VA, Shabaev AR, Frolov AV, Stasev AN, Lyapin AA, Kutikhin AG. EMbedding and Backscattered Scanning Electron Microscopy: A Detailed Protocol for the Whole-Specimen, High-Resolution Analysis of Cardiovascular Tissues. *Front Cardiovasc Med.* 2021;8:739549.

17. Han HC. Effects of material non-symmetry on the mechanical behavior of arterial wall. *J Mech Behav Biomed Mater.* 2022;129:105157.

18. Spears JR, Sinclair IN, Jenkins RD. Laser Balloon Angioplasty: Experimental In-Vivo and In-Vitro Studies. In: Lasers in Cardiovascular Medicine and Surgery: Fundamentals and Techniques; Editor: George S. Abela. Springer. 1990. pp:167-188.

19. King JB, Katta N, Teichman JMH, Tunnell JW, Milner TE. Mechanisms of Pulse Modulated Holmium:YAG Lithotripsy. *J Endourol.* 2021;35:S29-36.

20. McGarvey M, Kumar S, Violaris A, Elghamaz A, Salukhe TV, Yeh JS. Ventricular fibrillation induced by a lithotripsy-pulse on T during coronary intravascular shockwave lithotripsy. *Eur Hear J Case Rep.* 2020;4:1-3.

21. Curtis E, Khan A, El-Jack S, Glenie T. Precipitation of de novo atrial fibrillation during Shockwave Intravascular Lithotripsy® after pacing capture during the treatment of proximal right coronary artery disease: a case report. *Eur Hear J Case Rep.* 2019;3:1-4.

22. McQuillan C, Alkhalil M, Johnston PW. A paced heart without a pacemaker. *Eur Heart J.* 2019;40:819a.

23. Wilson SJ, Spratt JC, Hill J, Spence MS, Cosgrove C, Jones J, Strange JW, Halperin H, Walsh SJ, Hanratty CG. Incidence of "shocktopics" and asynchronous cardiac pacing in patients undergoing coronary intravascular lithotripsy. *EuroIntervention.* 2020;15:1429-35.

24. Beyder A, Rae JL, Bernard C, Strege PR, Sachs F, Farrugia G. Mechanosensitivity of Nav1.5, a voltage-sensitive sodium channel. *J Physiol.* 2010;588:4969-85.

25. Morris CE, Juranka PF. Nav channel mechanosensitivity: activation and inactivation accelerate reversibly with stretch. *Biophys J.* 2007;93:822-33.

26. Fitzgerald PJ, Ports TA, Yock PG. Contribution of localized calcium deposits to dissection after angioplasty. An observational study using intravascular ultrasound. *Circulation.* 1992;86:64-70.

27. Silva H, Tassone C, Ross EG, Lee JT, Zhou W, Nelson D. Collagen Fibril Orientation in Tissue Specimens From Atherosclerotic Plaque Explored Using Small Angle X-Ray Scattering. *J Biomech Eng.* 2022;144:024505.

28. Whelan A, Duffy J, Gaul RT, O'Reilly D, Nolan DR, Gunning P, Lally C, Murphy BP. Collagen fibre orientation and dispersion govern ultimate tensile strength, stiffness and the fatigue performance of bovine pericardium. *J Mech Behav Biomed Mater.* 2019;90:54-60.

29. Barrett HE, Van der Heiden K, Farrell E, Gijsen FJH, Akyildiz AC. Calcifications in atherosclerotic plaques and impact on plaque biomechanics. *J Biomech.* 2019;87:1-12.

30. Fujino A, Mintz GS, Matsumura M, Lee T, Kim SY, Hoshino M, Usui E, Yonetsu T, Haag ES, Shlofmitz RA, Kakuta T, Maehara A. A new optical coherence tomography-based calcium scoring system to predict stent underexpansion. *EuroIntervention.* 2018;13:e2182-e2189.

Supplementary data

Supplementary Appendix 1. Finite element analysis of pressure-lumen area relation.

Supplementary Table 1. Calcified coronary lesion characteristics.

Supplementary Table 2. Material coefficient for arterial wall and atherosclerotic plaque for finite element model studies.

Supplementary Figure 1. Balloon compliance.

Supplementary Figure 2. Scanning electron microscopy of *ex vivo* human coronary arteries.

The supplementary data are published online at: https://eurointervention.pcronline.com/doi/10.4244/EIJ-D-23-00487

Supplementary data

Supplementary Appendix 1. Finite element analysis of pressure-lumen area relation.

Simulation of the pressurized inflations were done using an FEA package (ABAQUS®). Arterial wall, atherosclerotic plaque and extracellular lipid (ECL) pools were meshed using eight-node linear brick reduced integration (C3D8R) elements. Both arterial wall and calcifications were assumed to be isotropic, incompressible, and hyperelastic material with polynomial strain energy density function. A uniform pressure up to 112 mmHg was gradually applied to the lumen mimicking balloon expansion. Both ends of the artery were free to expand radially but fixed in other directions. The material constants of the coronary arterial wall for the HGO model were determined by letting $\kappa = 0$ in equation (2) and refitted it to the mechanical behavior of coronary artery sample #2 given in the report. All material constants are given in supplemental Table S1. A constraint was used to eliminate the relative motion between contacting faces. In addition to the pre- and post-fractured models, more models with partial/complete de-bonding defined as the calcium plate separating from the surrounding tissue were simulated to determine how they would affect arterial compliance.

$$W = C_{10}(\bar{I}_1 - 3) + C_{20}(\bar{I}_1 - 3)^2 + C_{30}(\bar{I}_1 - 3)^3 + C_{40}(\bar{I}_1 - 3)^4 \quad (1)$$

Where $\bar{I}_1$ is the first invariant of deformation tensor and C_{10} to C_{40} are material constants. Medial and adventitial layers were assumed to be anisotropic, incompressible, and hyperelastic material with HGO strain energy density function.

$$W = \mu(\bar{I}_1 - 3) + \frac{k_1}{2k_2}\sum_{i=4,6}(\exp\{k_2\langle\kappa(\bar{I}_1 - 3) + (1 - 3\kappa)(\bar{I}_i - 1)\rangle^2\} - 1) \quad (2)$$

Where k_1, k_2, μ and κ are material constants, α represents fibre angle and $\bar{I}_i$ is the pseudo-invariant that reflects the stretch ratios in the two diagonal fibre directions.

Supplementary Table 1. Calcified coronary lesion characteristics.

Variable	400 µm fibre	230 µm fibre
number of arteries	15	4
maximum calcium angle, ^{0}	145 [66, 231]	215 [75, 342]
calcium thickness, mm	0.8 [0.36, 1.33]	0.6 [0.53, 0.72]
calcium length, mm	5.3 [1.6, 8.0]	6.3 [1.6, 14]
calcium score [30]	2 [0, 4]	4 [2, 4]
lumen gain, mm^2	1.4 [0.04, 8.64]	0.9 [0.4, 1.7]
compliance changes, %	53	NA

Supplementary Table 2. Material coefficient for arterial wall and atherosclerotic plaque for finite element model studies.

	C_{10} (MPa)	C_{20} (MPa)	C_{30} (MPa)	C_{40} (MPa)	
ECL pool	0.045	0.17	-0.13	0.11	
Ca^{2+}	0.21	64.86	-3.5e3	1.999e5	
	μ (MPa)	k_1 (MPa)	k_2	α	κ
Adventitia	0.26778e-3	1.531e-3	121.53	67.6	0
Media	0.436e-3	10.308e-3	5.93	25.8	0

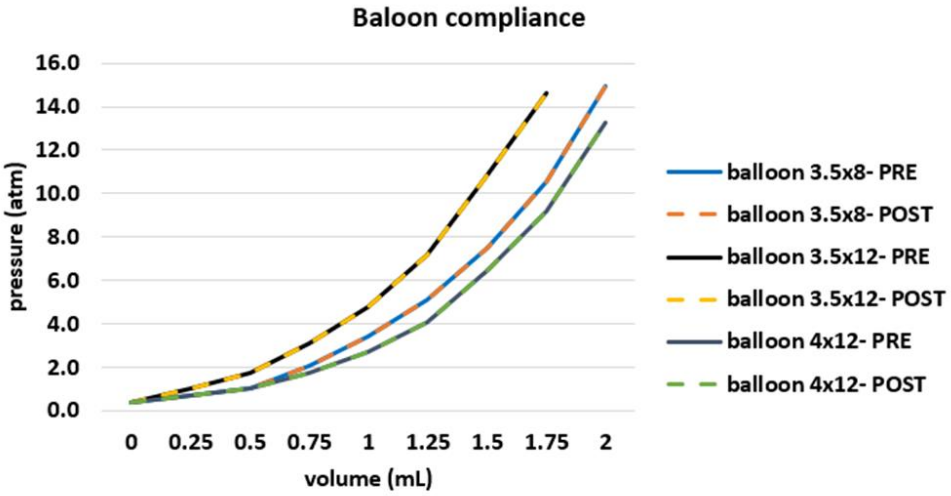

Supplementary Figure 1. Balloon compliance.

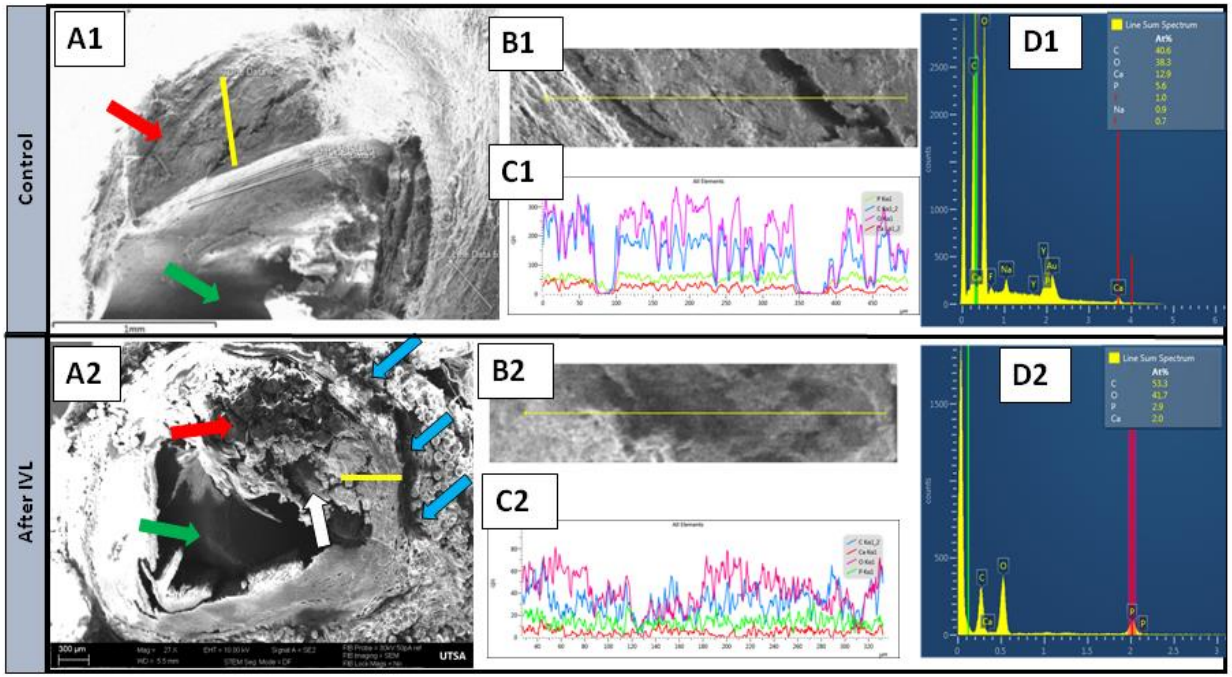

Supplementary Figure 2. Scanning electron microscopy of *ex vivo* human coronary arteries.

A. The cross section images of *ex vivo* human coronary artery (A1 – control region, A2 – region after laser IVL (red arrows calcific plaque, green arrow lumen, yellow line – spectroscopy sampling). B-D. Spectroscopy element analysis across atherosclerotic plaque (yellow line) in control (B1-C1) and treated (B2-C2) regions. The high calcium (Ca), phosphorus (P) and oxygen (O) content suggestive of a hydroxyapatite deposition in the plaque region (D1-D2).